

# 碳和氮元素对高强度奥氏体焊缝组织和性能的影响

张田宏, 杜 义, 张俊旭  
(洛阳船舶材料研究所, 河南 洛阳 471039)

摘 要: 采用扫描电镜(SEM)和透射电镜(TEM)等分析研究了碳、氮元素对奥氏体焊条熔敷金属组织和性能的影响。结果表明, 随着碳含量的增加, 熔敷金属晶界上 $M_{23}C_6$ 碳化物析出物逐渐增多, 析出颗粒增大, 虽然熔敷金属的抗拉强度有所提高, 但韧性明显降低。碳含量增加到一定程度后, 对强度的影响趋于平缓, 但对晶界碳化物的数量和尺寸仍然有强烈的促进作用, 韧性持续降低, 耐晶间腐蚀性能大大降低。随着氮含量的增加, 抗拉强度呈持续上升趋势, 同时韧性仍能保持在较高水平, 晶界上析出碳化物少, 抗晶间腐蚀性能良好。

关键词: 奥氏体焊条; 抗拉强度; 韧性; 碳化物

中图分类号: TG174 文献标识码: A 文章编号: 0253-360X(2007)07-081-05



张田宏

## 0 序 言

为了减少结构重量, 增大结构承载能力并提高机动性, 现代舰船结构的设计和建造大量采用调质状态的高强度高韧性船体结构钢, 在调质状态下焊接时, 为防止焊接冷裂纹, 常规的焊接工艺必须采用焊前预热、焊后热处理等措施, 并且严格控制层间温度<sup>[1]</sup>。预热和后热将带来降低生产效率、增加焊接施工费用和难以保证焊接质量等方面的问题。为了得到安全运行的焊接结构, 减少氢致冷裂纹的产生, 奥氏体焊接材料成为船体大刚性结构重要部位焊接的首选<sup>[2]</sup>。

焊接结构用船体高强度钢的强度水平一直在攀升, 目前奥氏体焊接材料的强度水平难以适应高强度船体钢的发展。因此, 有必要开发高强度级别的奥氏体焊接材料。

在奥氏体金属的强化方面, 固溶强化一直是人们研究的重点, 而碳和氮是对固溶强化贡献较大的主要元素, 作者以 705 MPa 级 A557 纯奥氏体不锈钢焊条为基础, 研究了元素碳和氮对高强度奥氏体焊条熔敷金属强度、韧性和耐晶间腐蚀性能的影响, 并结合微观组织观察, 探讨了碳、氮元素的作用机理。

## 1 试验材料和试验方法

试验以 A557 纯奥氏体不锈钢焊条为基础, 分别

向熔敷金属过渡不同含量的碳、氮来讨论碳、氮元素对熔敷金属组织和性能的影响。得到的不同含碳量和含氮量的熔敷金属化学成分如表 1 所示。

表 1 熔敷金属的化学成分(质量分数, %)

Table 1 Chemical composition of deposited metal

试样编号	C	Cr	Ni	N
C1	0.068	17.59	22.62	0.195
C2	0.079	17.38	21.91	0.194
C3	0.084	17.23	21.53	0.205
C4	0.090	17.72	22.04	0.217
C5	0.108	17.56	21.18	0.212
C6	0.120	18.19	21.84	0.196
C7	0.142	18.61	22.03	0.196
N1	0.072	18.02	23.18	0.194
N2	0.060	18.13	22.42	0.214
N3	0.067	18.40	22.13	0.226
N4	0.072	17.64	22.86	0.236
N5	0.071	18.46	22.32	0.244

在不同碳含量的 7 种(C1~C7)焊条熔敷金属中, 除碳含量达到了预期的变化目标外, 同样有着固溶强化作用的氮其含量有 0.023% 的波动; 在不同氮含量的 5 种(N1~N5)焊条熔敷金属中, 碳含量也有着 0.012% 的波动, 这些可能会对强度有一定影响, 但由于波动范围不大, 不会对试验结果有本质的影响。

采用 JSM-35C 扫描电镜及 DX-4X-ray 能谱仪对冲击断口形貌、夹杂物形态和分布以及断口夹杂物及析出物的成分进行观察和分析; 利用

Philips CM200 透射电镜对熔敷金属进行组织形貌和析出物观察,并运用选区电子衍射技术对析出物进行分析。晶间腐蚀检验按国家标准 GB/T4334.5—2000《不锈钢硫酸—硫酸铜腐蚀试验方法》进行,试样在微沸的硫酸—硫酸铜溶液中煮沸 16 h 后将试样弯曲 180° 来判断是否具有晶间腐蚀倾向。

## 2 试验结果与分析

### 2.1 熔敷金属的力学性能

对 C1~C7 和 N1~N5 几种焊条的熔敷金属分别进行了熔敷金属化学成分对力学性能的影响分析, C1~C7 焊条碳含量对力学性能的影响如图 1 所示, N1~N5 焊条氮含量对力学性能的影响如图 2 所示。

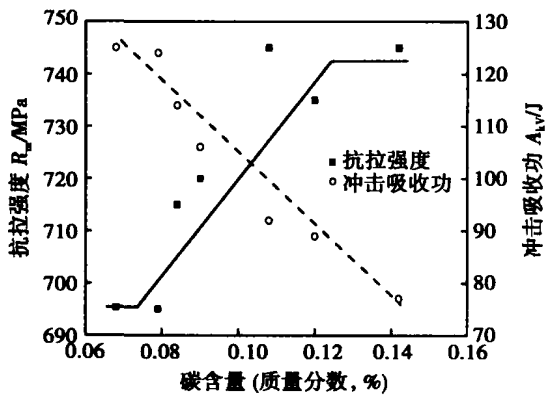


图 1 碳含量对熔敷金属力学性能的影响

Fig. 1 Effect of carbon content on mechanical properties of deposited metal

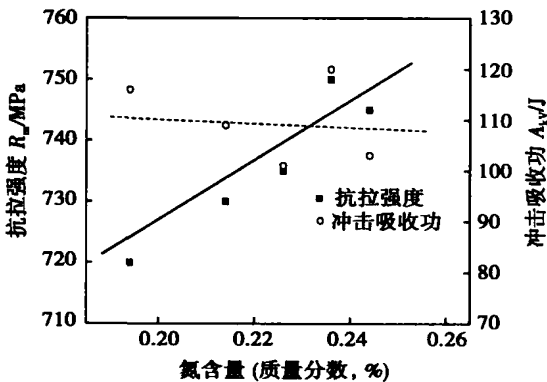


图 2 氮含量对熔敷金属力学性能的影响

Fig. 2 Effect of nitrogen content on mechanical properties of deposited metal

由图 1 和图 2 可以看出,不论是熔敷金属中碳含量的增加还是氮含量的增加,熔敷金属抗拉强度都呈现上升趋势(图中实线所示)。当碳含量增加到

一定程度(大于 0.10%)后,强度变化趋势减缓,而熔敷金属冲击吸收功随着碳含量的增加大幅度下降(图 1 中虚线所示),即使强度变化趋势减缓后,韧性仍继续降低;氮含量的增加对冲击吸收功影响很小,通过增加氮含量来提高抗拉强度后,熔敷金属的韧性仍能保持在较高水平。

### 2.2 熔敷金属冲击断口 SEM 形貌

对典型碳含量的 C1, C5, C7 焊条,以及氮含量最高的 N5 焊条熔敷金属冲击断口进行了扫描电镜分析。如图 3~图 5 所示, C1, C5, C7 焊条熔敷金属

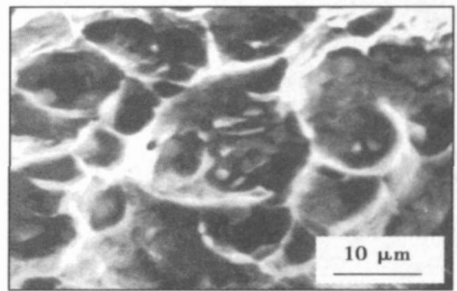


图 3 C1 焊条(C 元素含量 0.068%)冲击试样断口形貌  
Fig. 3 Fracture surface of charpy impact test sample with 0.068% C

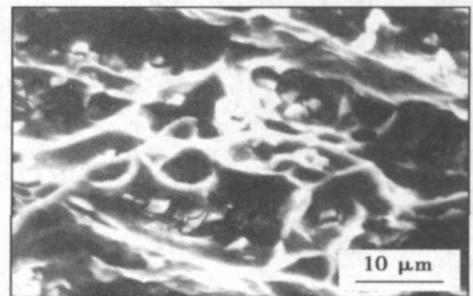


图 4 C5 焊条(C 元素含量 0.108%)冲击试样断口形貌  
Fig. 4 Fracture surface of charpy impact test sample with 0.108% C

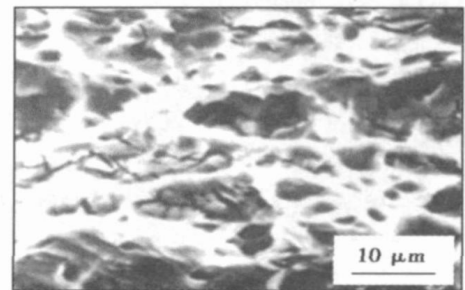


图 5 C7 焊条(C 元素含量 0.142%)冲击试样断口形貌  
Fig. 5 Fracture surface of charpy impact test sample with 0.142% C

断口形貌都呈现韧窝特征,在高倍镜下可见韧窝底部含有块状或片状脆性相。随着碳含量的增加,韧窝变浅,且韧窝由等轴晶状态向方向性的树枝晶状态发展,脆性相数量明显增多,脆性相的形态也从较独立的小颗粒逐渐呈大块状向连成片的形态发展。能谱分析结果表明,脆性相为富铬相。N5 焊条熔敷金属冲击断口形貌呈现韧窝特征,高倍镜下可见韧窝内夹杂物与脆性相很少(图 6)。

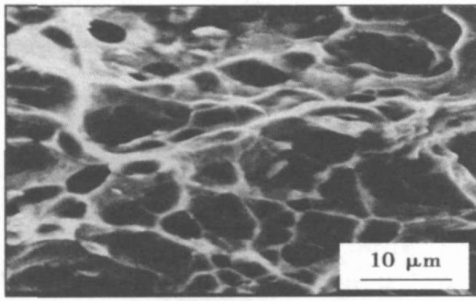


图 6 N5 焊条(N 元素含量 0.244%)冲击试样断口形貌  
Fig 6 Fracture surface of charpy impact test sample with 0.244%N

### 2.3 熔敷金属 TEM 组织分析

对 C1, C5, C7 焊条,以及 N5 焊条的熔敷金属进行了透射电镜组织分析。

C1 试样在所见范围内发现少量晶界上有碳化物析出,衍射分析表明,析出的碳化物为  $M_{23}C_6$  型,颗粒尺寸为 10~30 nm(图 7);C5 试样大部分晶界上有碳化物析出,此时析出物颗粒较大,直径约为 50~100 nm,部分晶界上碳化物连成较厚的薄膜,最宽处可达 150 nm,如图 8 所示,电子衍射分析的结果表明析出物属于  $M_{23}C_6$  型碳化物,电子衍射斑点(图 8a)

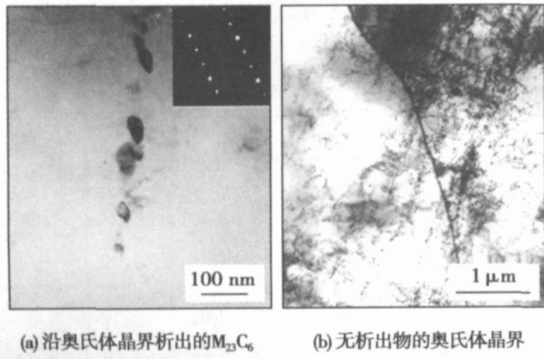


图 7 C1 焊条(C 元素含量 0.068%)熔敷金属 TEM 显微组织  
Fig. 7 TEM microstructures of deposited metal with 0.068% C

显示  $M_{23}C_6$  与奥氏体之间存在立方/立方取向关系,即  $\{111\}M_{23}C_6 // \{111\} \gamma$ ;  $\langle 011 \rangle M_{23}C_6 // \langle 011 \rangle \gamma$ ,这说明晶界上的  $M_{23}C_6$  是从奥氏体中析出的。C7 试样所见晶界上都有  $M_{23}C_6$  碳化物的析出,析出物颗粒直径约为 50~100 nm(图 9)。总的来说,随着碳含量的增加,有碳化物析出的晶界增多,且碳化物颗粒逐渐增大且沿晶界由碳化物颗粒连成薄膜。

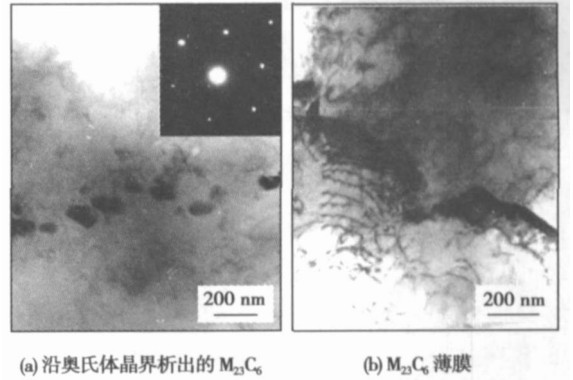


图 8 C5 焊条(C 元素含量 0.108%)熔敷金属 TEM 显微组织  
Fig 8 TEM microstructures of deposited metal with 0.108% C

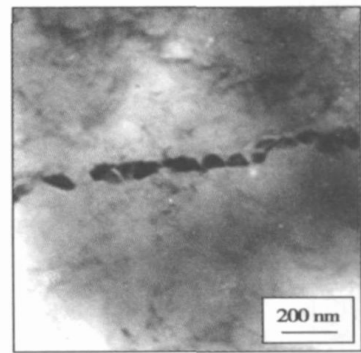


图 9 C7 焊条(C 元素含量 0.142%)熔敷金属 TEM 显微组织  
Fig 9 TEM microstructures of deposited metal with 0.142% C

在 N5 焊条熔敷金属试样中(图 10),观察到的整个界面上完全为单一奥氏体和析出物很少的晶界;在这样的氮含量范围内,熔敷金属中没有氮化物的析出和气孔的产生,说明此含量的氮能够全部固溶到奥氏体中。

### 2.4 熔敷金属的晶间腐蚀性能

对试验焊条熔敷金属进行的晶间腐蚀试验结果表明,C1 焊条和 N1~N5 焊条抗晶间腐蚀性能良好,其它焊条熔敷金属经过敏化处理弯曲 180° 都发生了不同程度的晶间腐蚀破坏。

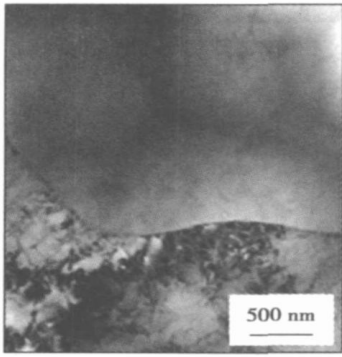


图 10 N5 焊条(N 元素含量 0.244%)熔敷金属 TEM 组织  
Fig. 10 TEM microstructures of deposited metal with 0.244% N

### 3 讨 论

奥氏体晶粒对碳具有很好的溶解性,但是,由于铬元素具有强烈的形成  $M_{23}C_6$  碳化物倾向,使得碳在奥氏体中活性降低,其高溶解度被大打折扣。随着含碳量的增加,虽然能够在一定程度上提高固溶强化的程度,但多余的碳以铬—铁碳化物的形式析出,主要是  $M_{23}C_6$ ,也有少量的以  $M_7C_3$  或  $M_6C$  的形式析出<sup>[3]</sup>。在试验中,碳含量高的熔敷金属晶界上析出的碳化物主要为  $M_{23}C_6$ 。 $M_{23}C_6$  的存在,降低了界面结合能,致使晶界强度下降,损害了焊缝金属的韧性,特别是晶界处碳化物随焊缝金属流动逐渐形成纤维组织,使焊缝的性能呈现方向性,此时,横向塑性指标显著降低;另一方面,由于碳化物中的含铬量是焊缝的 2~4 倍,而碳化物主要沿晶界析出,这导致了晶界的周围产生贫铬现象,其铬含量小于其耐腐蚀的最低极限 11.5%<sup>[4]</sup>,晶间腐蚀沿贫铬的晶界扩展,减弱了晶粒间的连接。

除碳以外,氮也是奥氏体不锈钢中最有效的固溶强化元素。近 10 年的研究表明,氮的大量加入可使奥氏体不锈钢达到非常高的强度。Pickering 等人<sup>[5]</sup>将 88 种不同奥氏体不锈钢的合金成分同强化机制联系起来,回归出下面的预测奥氏体不锈钢强度的方程,即

$$R_{p0.2} = [29 + 35(\%C) + 55(\%N) + 2.4(\%Si) + 1.2(\%Mo) + 5.0(\%Nb) + 3.0(\%Ti) + 1.2(\%Al) + 0.11(\%Ni) + 0.14(\% \delta\text{-铁素体}) + 0.82 \text{ 孪晶间距}] \times 15.4. \quad (1)$$

根据奥氏体不锈钢强度的回归方程式(1)可以看出,在奥氏体不锈钢中,氮的强化能力约为碳的 1.6 倍、钛的 18 倍、钼的 45 倍,氮在奥氏体中的固溶,强烈增加了焊缝金属的强度。在文中试验条件

下,氮含量变化范围为 0.05%,抗拉强度增加了约 30 MPa。

氮与碳虽然在钢中都是以间隙溶质原子形式出现,但占据着不同的晶格位置,氮原子更易于在固溶体中均匀分布,同时,氮原子比碳原子在奥氏体不锈钢中溶解度高,所以氮在奥氏体中不易形成脆性相。另一方面,有研究表明,氮含量的增加可以抑制奥氏体不锈钢中  $M_{23}C_6$  的析出<sup>[6]</sup>。从热力学上看,在铁基固溶体里,碳趋向于长程有序,促进了置换原子偏聚,导致形成晶界  $M_{23}C_6$  碳化物,而氮提供短程的原子有序,这种短程有序促进了更均匀的原子分配并延迟了氮化物的析出及长大,短程有序有利于合金元素更均匀地分布,增加了奥氏体不锈钢的稳定性,抑制了沉淀析出和发生腐蚀<sup>[7]</sup>。N1~N5 焊条碳含量较低,主要依靠氮的固溶作用进行强化,两方面因素的共同影响,晶界上形成的碳化物显著减少,防止了晶间腐蚀的发生。

### 4 结 论

(1) 碳含量对奥氏体焊条熔敷金属的强度和韧性有明显的影响,随着碳含量增加,抗拉强度显著提高,韧性明显降低。碳含量增加到一定程度后,对强度的影响趋于平缓,但韧性持续降低。

(2) C 元素含量在 0.068%~0.142%之间时,奥氏体焊条熔敷金属中均有  $M_{23}C_6$  型碳化物在晶界上析出,析出的数量和形态与碳含量有关。碳含量较低时,仅在少数晶界上有颗粒状碳化物析出,且颗粒较为细小;碳含量较高时,多数晶界上有碳化物析出,颗粒较大,且逐渐形成薄膜,熔敷金属的耐晶间腐蚀性能受到损害。

(3) 随着氮含量的增加,奥氏体焊条熔敷金属的抗拉强度显著提高,同时韧性仍能保持在较高的水平,晶界上碳化物析出极少,熔敷金属的抗晶间腐蚀性能良好。

### 参考文献:

- [1] Deloach J J, Null C, Fiore S, *et al.* The right welding wire could help the U. S. navy save millions[J]. *Welding Journal*, 1999, 78(6): 55-58.
- [2] Murti V S R, Sastry Y R, Rao V G N, *et al.* Some studies on the service weldability of HSLA steels using 18Cr, 8Ni, 6Mn type austenitic electrodes[J]. *Journal of Materials Processing Technology*, 1993, 37: 759-765.
- [3] Mcpherson N A, Chi K, Baker T N. Submerged arc welding of stainless steel and the challenge from the laser welding process[J]. *Journal*

解理论和析氢腐蚀理论来解释。

### 3 结 论

(1) 在 0.5 mol/L  $\text{Na}_2\text{CO}_3$ +1 mol/L  $\text{NaHCO}_3$  溶液中, 随着外加电位的正向增大, X80 管线钢焊接接头试样的断裂寿命、断面收缩率和应变量明显增加, 断口 SCC 的裂纹平均扩展速率降低, SCC 敏感性降低。

(2) 焊接接头试样在不同外加电位下进行慢应变速率试验后, 断口形貌在阴极电位条件下呈准解理断裂, 在自腐蚀电位和阳极电位条件下, 焊接接头试样断口主要以韧性断裂为主。

(3) X80 管线钢的应力腐蚀是阳极溶解和析氢腐蚀共同作用的结果。

#### 参考文献:

- [1] Rebak R B, Xia Z, Safruddin R, *et al.* Effect of solution composition and electrochemical potential on stress corrosion cracking of X-52 pipeline steel[J]. Corrosion, 1996, 52(5): 396-405.
- [2] Parkins R N, Belhimer E, Blanchard W K. Stress corrosion cracking of Materials Processing Technology, 2003 134: 174-179.
- [4] Erich Folkhard. 不锈钢焊接冶金[M]. 栗卓新, 朱学军, 译. 北京: 化学工业出版社, 2004.
- [5] Pickering F B. Some beneficial effects of nitrogen in steel[C] // Conference HNS-88, Lille, France, May 18-20, 1988. The Institute of Metals London 1989.
- [6] Schino A D, Kenny J M. Grain refinement strengthening of a microcrystalline high nitrogen austenitic stainless steel[J]. Materials Letters, 2003, 57: 1830-1834.

characteristics of a range of pipeline steels in carbonate-bicarbonate solution[J]. Corrosion, 1993, 49(12): 951-966.

- [3] Parkins R N. Mechanistic aspects of intergranular stress corrosion cracking of ferritic steels[J]. Corrosion, 1996, 52(5): 363-374.
- [4] 闫茂成, 翁永基. 环境溶液对管道应力腐蚀过程电化学行为的影响[J]. 中国腐蚀与防护学报, 2005, 25(1): 34-38.
- [5] 李明星, 王 荣, 李鹏亮, 等. X70 管线钢在模拟土壤介质中裂纹扩展量化模型[J]. 中国腐蚀与防护学报, 2004, 24(3): 163-167.
- [6] Delanty B O' Beime J. Major field study compares pipeline SCC with coatings[J]. Oil Gas Journal, 1992, 90(24): 39-44.
- [7] Blengino J M, Keddam M, Labbe J P, *et al.* Physico-chemical characterization of corrosion layers formed on iron in soditum carbonate-bicarbonate containing environment[J]. Corrosion Science, 1995, 37: 621-643.
- [8] 方丙炎, 王俭秋, 朱自勇, 等. 埋地管线在近中性 pH 和高 pH 环境中的应力腐蚀开裂[J]. 金属学报, 2001, 37(5): 453-458.
- [9] 王炳英, 霍立兴, 张玉凤, 等. X80 管线钢焊接接头的硫化氢应力腐蚀试验研究[J]. 压力容器, 2006, 23(7): 15-18.
- [10] 黄春波, 李光福, 杨 武. X70 管线钢焊缝应力腐蚀破裂的研究[J]. 腐蚀与防护, 2005 26(1): 1-5.

**作者简介:** 王炳英 女, 1972 年出生, 副教授, 博士研究生。主要研究方向为材料强度与断裂研究。发表论文 10 篇。

Email: tdwby2004@126.com

#### [上接第 84 页]

- [4] Erich Folkhard. 不锈钢焊接冶金[M]. 栗卓新, 朱学军, 译. 北京: 化学工业出版社, 2004.
- [5] Pickering F B. Some beneficial effects of nitrogen in steel[C] // Conference HNS-88, Lille, France, May 18-20, 1988. The Institute of Metals London 1989.
- [6] Schino A D, Kenny J M. Grain refinement strengthening of a microcrystalline high nitrogen austenitic stainless steel[J]. Materials Letters, 2003, 57: 1830-1834.

- [7] Mudali U K, Baldev R. 高氮钢和不锈钢——生产、性能与应用[M]. 李 晶, 黄运华, 译. 北京: 化学工业出版社, 2006.

**作者简介:** 张田宏 女, 1975 年出生, 硕士, 高级工程师。主要从事船体结构钢及配套焊接材料的开发及应用研究工作。发表论文 10 余篇。

Email: vila\_zhang@tom.com

relationship between the energy density and the welding time was approximately linear. And the welding time as well as the axial shortening increased with the energy density. Furthermore increasing the energy density produced an increase in the temperature of the interface and also an increase in the flash generated during the welding process. The calculated data of the welding time and axial shortening during welding were in good agreement with the measured data.

**Key words:** inertia friction welding; GH4169 alloy; energy density; numerical simulation

#### Pulsed MIG welding equipment based on DSP control

YANG Wenjie, LIAO Ping (School of Materials Science and Engineering, Jiamusi University, Jiamusi 154007, Heilongjiang, China). p77—80

**Abstract:** The structure of pulsed MIG (metal inert-gas) welding equipment which adopts inverter technology using IGBT, is designed based on DSP chip TMS320F2812 and mainly used on aluminum alloys. Welding control system comprises hardware and software, using C language welding program, and it reduces difficulty of control system exploitation. Scheduling control, sampling disposal of feedback signals and digital PI modulation are achieved through program control, and this controls veraciously welding process. Experimental results validated that this welding equipment is character with high control precision and stability, it can obtain better appearance of weld.

**Key words:** pulsed metal inert-gas; digital signal processing; inverter

#### Effect of carbon and nitrogen on microstructure and properties of austenite weld metal

ZHANG Tianhong, DU Yi, ZHANG Junxu (Luoyang Ship Material Research Institute, Luoyang 471039, Henan, China). p81—84, 88

**Abstract:** Effect of carbon and nitrogen on microstructure and properties of austenite weld metal were studied by scanning electron microscope, transmission electron microscope and other methods. With increasing C content, the quantity of  $M_{23}C_6$  carbide particles at austenite grain boundaries increased and the size of  $M_{23}C_6$  enlarged. The tensile strength of deposited metal increased, however, the toughness decreased markedly. When the content of C increases to a high level, the solution strengthening effect doesn't express anymore, but the quantity and size of carbide particles formed at austenite grain boundaries is still increasing. The toughness and intergranular corrosion resistance decreased continuously. With increasing N content, tensile strength increased, at the same time, the toughness kept at high level. Owing to small quantity of carbide particles formed at austenite grain boundaries, intergranular corrosion resistance displayed good performance.

**Key words:** austenitic electrode; tensile strength; toughness; carbide

#### $CO_3^{2-} - HCO_3^-$ stress corrosion test of welded joint for X80 pipeline steel

WANG Bingying, HUO Lixing, ZHANG Yufeng,

WANG Dongpo (School of Material Science and Engineering, Tianjin University, Tianjin 300072, China). p85—88

**Abstract:** The susceptibility to stress corrosion cracking (SCC) of the welded joint of X80 pipeline steel in solution of 0.5 mol/L  $Na_2CO_3$  and 1mol/L  $NaHCO_3$  was investigated by means of slow strain rate testing (SSRT) and scanning electron microscope. The results showed that all tensile test specimens cracked in welded joint and heat affected zone (HAZ). The general tendency in the studied potential range was that with positive increasing of potential, reduction in area, fracture time and elongation of specimens increased, and mean crack growth rate of SCC and the susceptibility to SCC decreased. At cathodic potentials, obvious quasi-cleavage fracture was observed in the fracture area of specimens. At open circuit potential and anodic potential, ductile fracture was the common fracture pattern. The mechanism of the stress corrosion could be explained with anodic solution theory and hydrogen induced cracking.

**Key words:** X80 pipeline steel; welded joint; slow strain rate testing; stress corrosion crack

#### Numerical simulation of welding temperature distribution for Ni-base superalloy little section square tube

WANG Junheng, ZHANG Guangjun, GAO Hongming, WU Lin (State Key Laboratory of Advanced Welding Production Technology, Harbin Institute of Technology, Harbin 150001, China). p89—93

**Abstract:** The welding temperature field of Ni-based superalloy little-section rectangular tube is calculated by using non-contact model. After comparing the simulating results with the measuring ones it indicates big errors when applying this model to the temperature field of little section rectangular in welding simulation. By analyzing the relationship between little-section rectangular tube and welding positioner in the view of mechanic and thermal perspectives, the reason for the errors of simulating results is found out. Based on this reason, the contact model is presented. The heat transfer and stress analysis between little section rectangular tube and welding positioner are simulated by using direct constraints method, and then the laws of the temperature distribution are gotten. The experimental results show that a "T" shaped temperature-field distribution is formed in the vicinity of the weld. After cooling for a period of time, the temperature distribution of the weldments shows that a lower temperature region exists at both ends and a higher temperature region exists in the middle of the tube. The computed results are in good agreement with the experimentally measured results.

**Key words:** little-section rectangular tube; contact; direct constraints method; temperature field

#### Microstructures and crack resistance of armoured steel welded by $CO_2$ shielded arc welding

ZHU Xiaoying, TAN Wei, ZHAO Yang (National Key Laboratory for Remanufacturing, Academy of Armored Forces Engineering, Beijing 100072, China). p94—96

**Abstract:** The armoured steel welded joints were prepared by  $CO_2$  shielded arc welding with modified H10MnSi wire and H08Mn2Si wire respectively. The microstructures of the welded